materials

MDPI

Article

The Biofilm Inhibition Properties of Glucosamine Gold Nanoparticles in Combination with Meropenem against *Pseudomonas aeruginosa* on the Endotracheal Tube: A Model of Biofilm-Related Ventilator-Associated Pneumonia

Dewi Santosaningsih [1,2,*], Yuanita Mulyastuti [1], Soeyati Poejiani [1], Rilia F. Putri [3], Liliana Dewi [4], Hisanifa Arifani [4], Yatim L. Ni'mah [5] and Afaf Baktir [6,*]

1 Department of Clinical Microbiology, Faculty of Medicine, Universitas Brawijaya, Malang 65142, Indonesia; yuanmic@ub.ac.id (Y.M.); ucik.fk@ub.ac.id (S.P.)
2 Department of Clinical Microbiology, Dr. Saiful Anwar Hospital, Malang 65112, Indonesia
3 Magister of Chemistry Study Program, Faculty of Science and Technology, Universitas Airlangga, Surabaya 60115, Indonesia; rilia.faradini.putri-2023@fst.unair.ac.id
4 School of Medicine, Faculty of Medicine, Universitas Brawijaya, Malang 65142, Indonesia; lilyanaad10@student.ub.ac.id (L.D.); hisanifaarifani@student.ub.ac.id (H.A.)
5 Department of Chemistry, Faculty of Science and Data Analytics, Institut Teknologi Sepuluh Nopember, Surabaya 60111, Indonesia; yatimnikmah@gmail.com
6 Department of Chemistry, Faculty of Science and Technology, Universitas Airlangga, Surabaya 60115, Indonesia
* Correspondence: dewi.santosa@ub.ac.id (D.S.); afafi2001@yahoo.com (A.B.)

Abstract: Biofilm-related infections play a significant role in the development and persistence of ventilator-associated pneumonia. *Pseudomonas aeruginosa* (*P. aeruginosa*) frequently causes biofilm-related infections associated with ventilator tubing. Glucosamine gold nanoparticles (AuNPs) may exhibit antibiofilm properties; however, more studies, including combinatorial therapy with antibiotics, are needed to explore their potential applications in clinical settings. This study aims to investigate the biofilm inhibition properties of glucosamine AuNPs in combination with meropenem against *P. aeruginosa* ATCC 9027 on the endotracheal tube. A biofilm inhibition assay of glucosamine AuNPs at 0.02 mg/mL, both singly and in combination with meropenem at 1 mg/mL, was carried out against *P. aeruginosa* ATCC 9027 on an endotracheal tube using the tissue culture plate method. Scanning electron microscopy was performed for visualization. Glucosamine AuNPs at 0.02 mg/mL combined with meropenem at 1 mg/mL showed greater biofilm inhibition (72%) on the endotracheal tube than glucosamine nanoparticles at 0.02 mg/mL alone (26%) (p = 0.001). The scanning electron microscopic visualization revealed that the untreated *P. aeruginosa* biofilm was denser than the glucosamine nanoparticles-treated biofilm, whether combined with meropenem or using glucosamine nanoparticles alone. The combination of glucosamine AuNPs and meropenem may have the synergistic effect of inhibiting biofilm production of *P. aeruginosa* on the endotracheal tubes of patients with mechanical ventilation. Conducting additional experiments to explore the impact of combining glucosamine-coated gold nanoparticles (AuNPs) with meropenem on the inhibition of biofilm production by clinical *P. aeruginosa* isolates would be beneficial.

Keywords: biofilm; glucosamine nanoparticles; *Pseudomonas aeruginosa*

Citation: Santosaningsih, D.; Mulyastuti, Y.; Poejiani, S.; Putri, R.F.; Dewi, L.; Arifani, H.; Ni'mah, Y.L.; Baktir, A. The Biofilm Inhibition Properties of Glucosamine Gold Nanoparticles in Combination with Meropenem against *Pseudomonas aeruginosa* on the Endotracheal Tube: A Model of Biofilm-Related Ventilator-Associated Pneumonia. *Materials* **2024**, *17*, 1604. https://doi.org/10.3390/ma17071604

Academic Editor: Eugen Gheorghiu

Received: 7 December 2023
Revised: 27 March 2024
Accepted: 27 March 2024
Published: 31 March 2024

1. Introduction

Biofilm infections involving *Pseudomonas aeruginosa* (*P. aeruginosa*) present a complex and persistent problem in clinical settings [1,2]. As an opportunistic pathogen, *P. aeruginosa* is known for its remarkable ability to form robust biofilms, which are organized groups of bacteria surrounded by a matrix they produce themselves [3–5]. This matrix

provides essential structural support and protection, enabling the bacteria to adhere to surfaces, evade hosts' immune responses, and exhibit resistance to conventional antimicrobial therapies [5,6].

The challenges posed by *P. aeruginosa* biofilm infections are multifaceted. One key challenge is the inherent antibiotic resistance displayed by bacteria within biofilms. This resistance is attributed to limited drug penetration into the biofilm matrix and the altered physiological states of bacteria residing within the biofilm [7]. Consequently, conventional antibiotic treatments often prove ineffective against biofilm-associated infections [2].

A notable aspect of *P. aeruginosa* biofilm infections is their association with medical devices, such as catheters, implants, and ventilator tubes [8–11]. These devices provide ideal surfaces for biofilm formation, leading to impaired device function and an elevated risk of systemic infections [12]. Biofilm formation on ventilator tubes poses a serious risk in healthcare settings, leading to ventilator-associated pneumonia, as well as increased patient morbidity and healthcare costs [11]. Research efforts are being made that are dedicated to unraveling the molecular mechanisms underlying *P. aeruginosa* biofilm formation and investigating potential targets for therapeutic intervention [13–15]. Understanding the roles of quorum sensing, extracellular polymeric substance (EPS) production, and other virulence factors is paramount in devising effective strategies to disrupt biofilm development [15].

Nanoparticles have emerged as promising tools in the battle against biofilm formation due to their unique physicochemical properties and versatile applications. These nanoscale materials exhibit a range of effects that interfere with various stages of biofilm development, offering innovative strategies to combat this persistent problem and improve the efficacy of antimicrobial approaches. The effects of nanomaterials on preventing biofilm formation include physical disruption, surface modification, release of antimicrobials, disruption of quorum sensing, electrostatic interactions, mechanical stress, photothermal effects, and enzymatic degradation [16,17].

Gold nanoparticles (AuNPs) have attracted significant scientific and technological interest in the past few decades [17,18]. In comparison with other nanoparticles, AuNPs are recognized for their exceptional stability and have been synthesized in diverse shapes and structures. Additionally, they exhibit adjustable and distinctive optical properties [17,19,20]. Currently, AuNPs have been engineered for diverse applications in the medical and pharmaceutical domains. These applications encompass utilization of their antibacterial and antibiofilm properties, among others [20].

Glucosamine is a naturally occurring amino sugar that serves as a building block for various molecules within the body, including glycosaminoglycans (GAGs) and proteoglycans. In recent years, glucosamine nanoparticles have gained attention for their potential applications in various fields, including medicine and material science [15–17]. In the context of preventing biofilm formation, glucosamine nanoparticles have been investigated for their ability to inhibit initial bacterial adhesion. The functional groups on the surface of glucosamine can interact with bacterial cell surfaces, disrupting their attachment and colonization on surfaces. Additionally, glucosamine nanoparticles might interfere with the quorum sensing systems that play a role in biofilm formation by inhibiting bacterial communication [6,18].

Previous studies have reported the synergistic antibiofilm effect of colistin + meropenem against *Myroides odoratimimus*, and that of a combination of liquid crystal nanoparticles + tobramycin against *P. aeruginosa* [21,22]. León-Buitimea A. et al. described a potential combination therapy using antibiotics and other antimicrobial agents, including nanoparticles, to combat antibiotic-resistant bacteria [23]. The combination of antibiotics and AuNPs, particularly those functionalized with glucosamine, has the potential to exhibit synergistic antibiofilm effects. This approach involves leveraging the advantages of both antibiotics and AuNPs to enhance antibiofilm activity and overcome limitations associated with conventional antibiotic therapies. However, the effects of the conjugation of glucosamine phosphate and AuNPs (GlcN-AuNPs)—alone and in combination with meropenem—on *P. aeruginosa* biofilms are still unclear.

We aimed to investigate the effectiveness of GlcN-AuNPs, both alone and combination with meropenem, in preventing biofilm formation of *P. aeruginosa* ATCC 9027 on the endotracheal tube, serving as a model of ventilator-associated pneumonia. Ex vivo assessment of glucosamine nanoparticles' effectiveness against *P. aeruginosa* biofilm was conducted using the tissue culture plate method and scanning electron microscopy.

2. Materials and Methods

2.1. Endotracheal Tube Pieces Preparation

The package of endotracheal tube (Life Resources, Zhanjiang, China) was opened within the biological safety cabinet. The endotracheal tube was cut, with a sterile scalpel, to around 0.5 cm per piece. A piece of sterile endotracheal tube was placed into an individual well of tissue culture plate for further experiment [17].

2.2. Bacterial Isolate

P. aeruginosa ATCC 9027 was used in this study. The isolates from fresh agar plates were inoculated in 5 mL of trypticase soy broth (Oxoid, Basingstoke, UK) and were kept for incubation at 37 °C for 24 h. The inoculum, measured at 10^8 CFU/mL by spectrophotometry, was used for the biofilm formation assay on the endotracheal tube.

2.3. AuNPs Preparation

The preparation of AuNPs with average sizes of 10 nm was conducted as previously described, with slight modifications [24,25]. Briefly, 1 mL of 0.1% *m*/*v* $HAuCl_4.3H_2O$ and 49 mL water were added to 4 mL of 0.02%, 0.04%, and 0.06% (*m*/*v*) Na_3-citrate solution, with continuous stirring at 60 °C and 800 rpm for 45 min. Subsequently, the mixture was cooled to room temperature before the addition of glucosamine phosphate.

2.4. Conjugation of Glucosamine Phosphate and AuNPs (GlcN-AuNPs)

The different concentrations of GlcN-AuNPs were generated as previously described [25]. Appropriate amounts of glucosamine phosphate (Sigma-Aldrich, St. Louis, MO, USA) were added into a cylindrical flask with a flat bottom containing 5 mL of AuNPs at a designated flow rate (0.150 mL/min). The mixture was stirred at 800 rpm at room temperature. The final concentrations of GlcN-AuNPs were 0.008%, 0.012%, 0.016%, 0.020%, and 0.024%. Ultraviolet–visible spectrophotometry (ThermoScientific Genesys 150, Thermo Fisher Scientific, Waltham, MA, USA) and transmission electron microscopy (TEM) (JOEL JEM-1400, Peabody, MA, USA) of GlcN-AuNPs were performed prior to usage for characterization and quality assurance purposes. The TEM images were obtained at the TEM service unit in the Department of Chemistry, Faculty of Mathematics and Natural Sciences, Gadjah Mada University, Yogyakarta, Indonesia.

2.5. Ex Vivo Assessment of GlcN-AuNPs against P. aeruginosa ATCC 9027 Biofilms

The tissue culture plate method was carried out to investigate the biofilm formation of *P. aeruginosa* ATCC 9027 on the endotracheal tube pieces [26]. The effect of GlcN-AuNPs, either alone or in combination with meropenem, on early biofilms was evaluated. Therefore, the plates underwent a two-step incubation process [4].

Pieces of ETT were placed in individual wells of 24-well flat bottom polystyrene (Biologix Europe GmbH, Hallbergmoos, Germany). Individual wells of 24-well flat bottom polystyrene were filled with 200 µL of 10^8 CFU/mL *P. aeruginosa* ATCC 9027 inoculums and 200 µL trypticase soy broth–glucose medium. The uninoculated medium, serving as the negative control, was added to each well to ensure that the medium was sterile. After the plates were incubated for eight hours at 37 °C (first incubation), the broth medium was carefully pipetted out of the wells. Plates were washed twice with 200 µL of phosphate buffer saline (pH 7.2). The ETT was moved to new individual wells of 24-well flat bottom polystyrene. The individual wells were filled with 200 µL of trypticase soy broth (without glucose) for further experiments described in Table 1 [4].

Table 1. The ex vivo assessment of GlcN-AuNPs against *P. aeruginosa* biofilm.

Group	Treatment
1	*P. aeruginosa* ATCC 9027 (untreated)
2	*P. aeruginosa* ATCC 9027 + GlcN-AuNPs 0.02 mg/mL
3	*P. aeruginosa* ATCC 9027 + GlcN-AuNPs 0.02 mg/mL + meropenem 1 mg/mL

Plates then were incubated at 37 °C for 24 h (second incubation). After 24 h of incubation, plates were washed twice with 200 µL of phosphate buffer saline (pH 7.2) and incubated at 37 °C for an hour. The plates were stained with 200 µL of 0.1% crystal violet for 10 min. Excess stain was removed by washing twice with deionized water and the plates were kept for drying. Next, 200 µL of 33% glacial acetic acid was added to the wells. The optical densities (OD) of the isolates were determined using a micro-ELISA auto reader (BIORAD, Hercules, CA, USA) at a wavelength of 570 nm. The experiment was performed in quadruples per group. The analysis of optical density data for identifying biofilm formation is displayed in Table 2. Additionally, the percentage of biofilm inhibition was determined using the following formula [22]:

$$\% \text{ inhibition} = 100 - (\text{OD570 sample}/\text{OD570 untreated group} \times 100).$$

Table 2. Interpretation of optical density data for detection of biofilm formation [27].

Average OD Value	Interpretation
OD $\leq$ ODc	No biofilm formation
ODc < OD $\leq$ 2 $\times$ ODc	Weak biofilm formation
2 $\times$ ODc < OD $\leq$ 4 $\times$ Odc	Moderate biofilm formation
4 $\times$ ODc < OD	Strong biofilm formation

Notes: all OD values were measured at 570 nm; ODc = average OD of negative control + 3 $\times$ standard deviation of the negative controls; Odc = optical density cutoff value.

2.6. Quantification of Bacterial Biofilms

The quantification of bacterial biofilms was conducted as previously described [28]. Briefly, the biofilm was extracted from endotracheal tube (ETT) pieces using vortex and sonication. The sonicate was concentrated by centrifugation at 3100$\times$ *g* for 10 min and the resulting pellet was resuspended in 1 mL PBS. Serial dilutions, including neat sonicate, were plated on LB agar using the 20 µL drop method in triplicate and then incubated at 37 °C for 14–18 h. After incubation, the number of colonies per 20 µL drop was counted. The quantification of biofilm bacteria utilized the formula of CFU/cm = (average number of colonies for a dilution) $\times$ 50 $\times$ dilution factor.

2.7. Scanning Electron Microscope

Scanning electron microscope preparation was conducted following the previous described method [29]. Initially, the suspensions containing a piece of ETT in each well of the tissue culture microplate were discarded. Subsequently, each ETT piece underwent two gentle rinses with 1% sterile phosphate-buffered saline (Merck, Rahway, NJ, USA) and was fixed with 2.5% glutaraldehyde for 2 h. The fixed ETT pieces were then washed again with PBS and dehydrated through a series of graded ethanol solutions. Finally, the ETT pieces were removed from the wells, dried overnight, and coated in gold before imaging. The examination was performed using a scanning electron microscope (Hitachi TM 3000, Tokyo, Japan) at the Laboratory of Bioscience, Brawijaya University, Malang, Indonesia.

3. Results

3.1. Characterization of GlcN-AuNPs

Figure 1 displays the ultraviolet–visible spectra of both AuNPs and GlcN-AuNPs, revealing a distinctive absorption band in the range of approximately 500–550 nm. The AuNPs (0%) showed an absorption band at 525 nm; this presence signifies the formation of AuNPs. The functionalization of GlcN-AuNPs in different concentrations, including 0.008%, 0.012%, 0.016%, 0.020%, and 0.024% (*m*/*v*), resulted in similar absorption bands at 525 nm, reflecting the similar sizes, shapes, and surfaces of the nanoparticles. In addition, the morphologies and particle sizes of AuNPs and GlcN-AuNPs were characterized by TEM. Both AuNPs and GlcN-AuNPs were found to have a spherical shape and exhibited an average size of less than 100 nm (Figure 2).

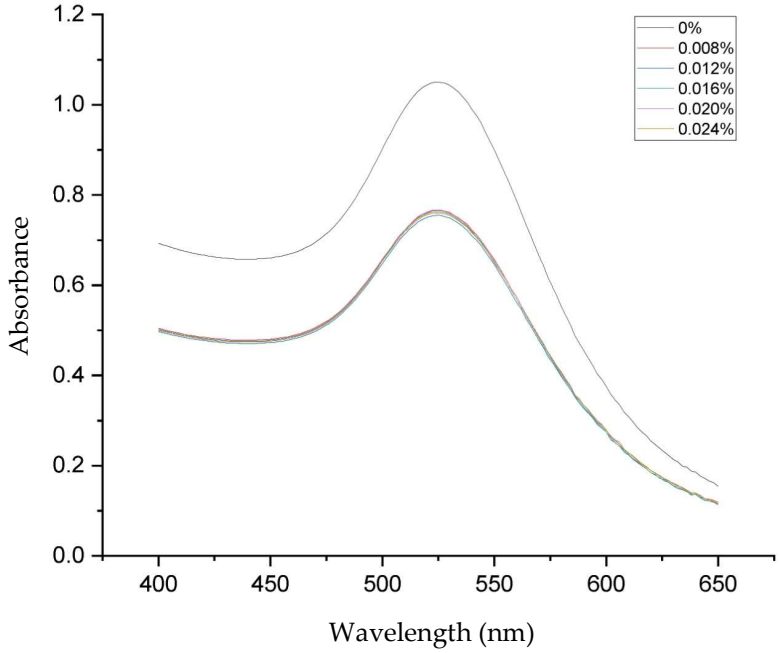

Figure 1. Visible absorption spectra for AuNPs without glucosamine (0%) and functionalization of GlcN-AuNPs in different concentrations (0.008%, 0.012%, 0.016%. 0.020%, and 0.024% *m*/*v*).

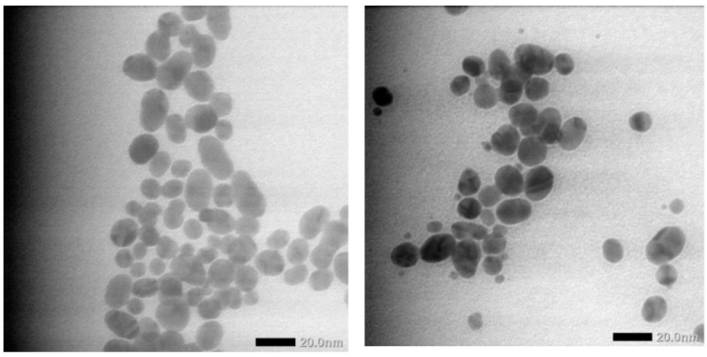

Figure 2. Transmission electron micrographs of (**A**) AuNPs and (**B**) GlcN-AuNPs showing size distributions and shapes.

3.2. Biofilm Formation of P. aeruginosa ATCC 9027 on an Endotracheal Tube

The detection of biofilm formation by *P. aeruginosa* ATCC 9027 on endotracheal tube pieces using the tissue culture plate method shows different intensities among treatment groups (Figure 3). In concordance with the interpretation of the optical density results

presented in Table 3, the untreated group (first row) showing high intensity indicates strong biofilm production. After exposure to GlcN-AuNPs alone and in combination with meropenem (second and third row), the intensity of biofilm formation by *P. aeruginosa* ATCC 9027 was lower, exhibiting moderate biofilm production.

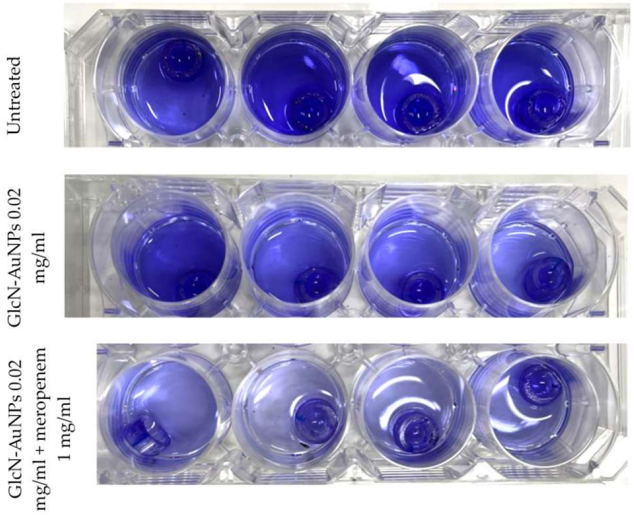

Figure 3. Detection of biofilm formation by *P. aeruginosa* ATCC 9027 on endotracheal tube pieces using tissue culture plate method (four replications per group) before acid was added.

Table 3. Biofilm activity assay of *P. aeruginosa* ATCC 9027 treated with GlcN-AuNPs.

Group	Replication	OD	Mean ± SD	Interpretation
Untreated	1	1.863	2.466 ± 0.406 [a]	Strong biofilm formation
	2	2.724		
	3	2.584		
	4	2.695		
GlcN-AuNPs 0.02 mg/mL	1	2.618	1.832 ± 0.601 [a]	Moderate biofilm formation
	2	1.887		
	3	1.648		
	4	1.176		
GlcN-AuNPs 0.02 mg/mL + meropenem 1 mg/mL	1	0.908	0.720 ± 0.173 [b]	Moderate biofilm formation
	2	0.533		
	3	0.620		
	4	0.819		

One-way ANOVA analysis: *p*-Value = 0.001, [a] and [b] indicate results that are significantly different according to Tukey's post-hoc test. OD = optical density; SD = standard deviation.

In addition, endotracheal tube pieces exposed to untreated *P. aeruginosa* ATCC 9027 demonstrated biofilm production, with the biofilm manifesting as confluent sheets of cells within a dense extracellular matrix observed by scanning electron microscopy (Figure 4A). In contrast, the negative control tube containing trypticase soy broth media showed no evidence of biofilm formation upon scanning electron microscopy examination (Figure 4D). Figure 4B displays the distribution of intact planktonic cells not covered by an extracellular matrix, indicating the inhibition of biofilm formation of *P. aeruginosa* ATCC 9027 after exposure to GlcN-AuNPs 0.02 mg/mL alone. The combination of GlcN-AuNPs 0.02 mg/mL and meropenem 1 mg/mL applied to the ETT pieces resulted in a simultaneous effect. The

SEM image shows damage to the planktonic cells, and the extracellular matrix sheet is absent (Figure 4C).

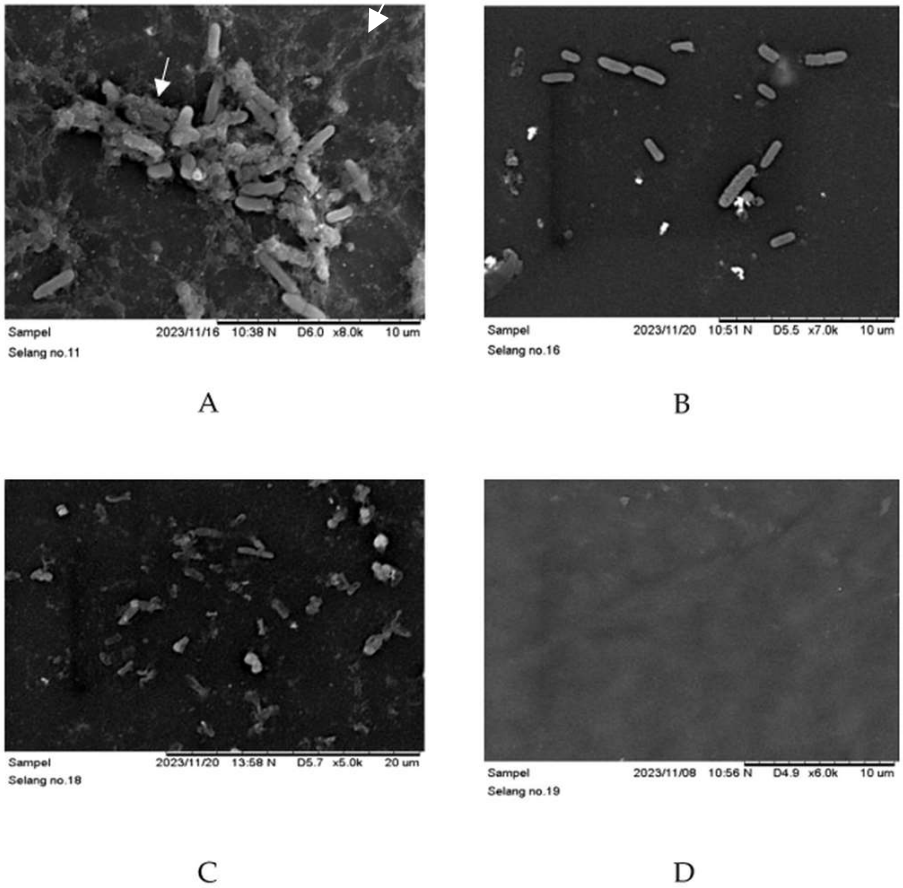

Figure 4. Biofilm formation of *P. aeruginosa* ATCC 9027 on endotracheal tube pieces, observed by scanning electron microscopy. (**A**) = untreated *P. aeruginosa* ATCC 9027; white arrow shows bacterial cells covered by extra polysaccharides matrix (**B**) = *P. aeruginosa* ATCC 9027 treated with GlcN-AuNPs 0.02 mg/mL alone; (**C**) = *P. aeruginosa* ATCC 9027 treated with GlcN-AuNPs 0.02 mg/mL + meropenem 1 mg/mL; (**D**) = negative control; white arrow shows bacterial cells covered by extrapolysaccharides matrix.

3.3. Biofilm Inhibition Activities of GlcN-AuNP, Both Alone and in Combination with Meropenem, against P. aeruginosa ATCC 9027 on the Endotracheal Tube

The results demonstrated a decrease in biofilm production of *P. aeruginosa* 9027 on the endotrachael tube after exposure to GlcN-AuNPs, either alone or in combination with meropenem (Figure 5). The percentage of biofilm inhibition was 26% and 71% after exposure to GlcN-AuNPs alone and in combination with meropenem, respectively. *P. aeruginosa* ATCC 9027 exhibited the lowest level of biofilm formation, significantly decreased after exposure to the combination of GlcN-AuNPs and meropenem (F value = 16.832; $p = 0.001$). The Tukey post-hoc test revealed a significant decrease in the biofilm formation level of *P. aeruginosa* 9027 when treated with the combination of GlcN-AuNPs and meropenem, compared to both the untreated group and those treated with GlcN-AuNPs alone (Table 3).

Quantification of *P. aeruginosa* ATCC 9027 biofilms on the cultivation media showed decreases in the colony-forming unit counts of bacterial biofilms after exposure to either GlcN-AuNPs 0.02 mg/mL alone (99%) or GlcN-AuNPs 0.02 mg/mL combined with meropenem 1 mg/mL (95%). However, the CFU count was not significantly different after exposure to GlcN-AuNPs 0.02 mg/mL alone compared to GlcN-AuNPs 0.02 mg/mL combined with meropenem 1 mg/mL ($p = 0.042$) (Table 4).

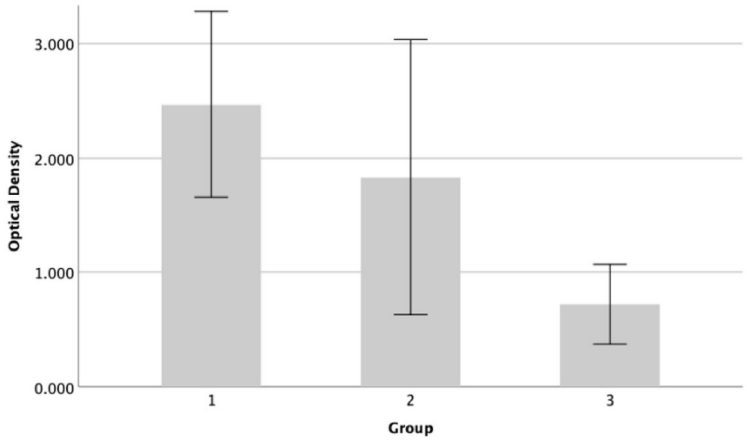

Figure 5. The biofilm-forming activity of *P. aeruginosa* ATCC 9027. The assessment of biofilm formation was conducted using the microtiter plate technique and staining with crystal violet. The graph displays the average ± standard deviation of biofilm formation derived from three groups. Group 1 = untreated; group 2 = GlcN-AuNP 0.02 mg/mL; group 3 = GlcN-AuNPs 0.02 mg/mL + meropenem 1 mg/mL.

Table 4. Quantification of bacterial biofilms from *P. aeruginosa* ATCC 9027 treated with GlcN-AuNPs on the surface of endotracheal tube pieces.

Group	Replication	CFU/cm	Mean ± SD
Untreated [a]	1	50.1×10^6	$46.4 \times 10^6 \pm 5.5 \times 10^6$
	2	49.1×10^6	
	3	40.1×10^6	
GlcN-AuNPs 0.02 mg/mL [b]	1	11.2×10^4	$44.0 \times 10^3 \pm 59.7 \times 10^3$
	2	2.0×10^4	
	3	0	
GlcN-AuNPs 0.02 mg/mL + meropenem 1 mg/mL [b]	1	54.1×10^3	$20.2 \times 10^5 \pm 19.7 \times 10^5$
	2	20.1×10^5	
	3	40.0×10^5	

Kruskal–Wallis analysis: *p*-Value = 0.042, [a] and [b] indicate results that are significantly different. CFU = colony-forming unit; SD = standard deviation.

4. Discussion

Ventilator-associated pneumonia is defined as pneumonia that develops in patients undergoing mechanical ventilation via an ETT for over 48 h in the hospital. The formation of a biofilm on the ETT significantly contributes to the occurrence of VAP [11]. This type of pneumonia affects 25–56% of all mechanically ventilated patients [30].

Ventilator-associated pneumonia is mainly caused by multidrug-resistant and extremely drug-resistant strains of *P. aeruginosa*, leading to high rates of treatment failure. The effectiveness of antibiotics such as aminoglycosides, quinolones, and β-lactams are limited by the rapid formation of *P. aeruginosa* biofilms on endotracheal tubes, which are a crucial virulence factor and make bacterial elimination more challenging [31,32].

Meropenem, a β-lactam antibiotic, is highly effective against multidrug-resistant *P. aeruginosa* [29]. Nevertheless, there is a global trend of increased carbapenem resistance among these organisms [33].

Nanomaterials with strong antimicrobial properties are potential alternatives to conventional antibiotics, as they bypass common antibiotic resistance mechanisms [34]. They inhibit biofilm formation through various mechanisms such as physical disruption, surface modification, antimicrobial release, interference with quorum sensing, electrostatic

interactions, mechanical stress, photothermal effects, and enzymatic degradation [16,17]. In addition, there have been reports on the synergistic effect of combining nanomaterials with antibiotics to prevent biofilm formation [23]. A prior study documented the benefit of the antimicrobial and antibiofilm effects of meropenem and ZnO nanoparticles in protecting a cornea rat model from pseudomonas-induced keratitis [29].

To our knowledge, this study is the first to experiment with synthesizing glucosamine phosphate with gold nanoparticles (GlcN-AuNPs) and applying the resulting material simultaneously with meropenem to inhibit biofilm formation on the endotracheal tube. Gold nanoparticles are recognized for their significant potential in biomedical applications, including drug delivery, imaging, and diagnostics, due to their ease of preparation, surface reactivity, and unique optical properties [35]. Gold is a generally non-toxic nanomaterial; however, the substances employed in its preparation and modification may have toxic properties. However, at specific concentrations, gold nanoparticles exhibit antibacterial effects without toxicity to normal cells [19]. In addition, the compact size of AuNPs and their biocompatibility with biological systems, minimal toxicity, and ability to combine different molecular functionalities simultaneously make them attractive for use in biomedical applications involving therapy and sensing [35].

In this study, we found that AuNPs conjugated with glucosamine phosphate effectively inhibited biofilm formation by *P. aeruginosa* ATCC 9027 on the endotracheal tube. This finding is consistent with a previous study that highlighted the effectiveness of AuNPs in combating biofilm-related infections caused by *P. aeruginosa* PAO1 [36]. Experimental evidence suggests that the glucose subunit in glucosamine phosphate plays a crucial role, stimulating the generation of intracellular NAG-6-P, which inactivates the regulator NagC and reduces biofilm formation [37,38].

Moreover, this study demonstrated that combining GlcN-NPs and meropenem effectively reduced biofilm formation by *P. aeruginosa* ATCC 9027 on the endotracheal tube. The combination was nearly three times more effective than GlcN-NPs alone (Figure 5). The statistical analysis, using Tukey's post-hoc test, revealed no significant difference in mean optical density between the untreated group ($p = 2.466 \pm 0.406$) and GlcN-AuNP 0.02 mg/mL ($p = 1.832 \pm 0.601$). However, a significant difference was observed between the untreated group and GlcN-AuNPs 0.02 mg/mL + meropenem 1 mg/mL ($p = 0.720 \pm 0.173$). The combination of nanomaterials and antibiotics could potentially contribute to enhancing the activity of biofilm inhibition against *P. aeruginosa* ATCC 9027 [29]. Nevertheless, further research is needed to understand the impact of GlcN-AuNPs and meropenem on clinical *P. aeruginosa* isolates from mechanically ventilated patients.

The quantification of bacterial biofilms showed that either GlcN-NPs alone or GlcN-AuNPs 0.02 mg/mL combined with meropenem 1 mg/mL could reduce the bacterial load of *P. aeruginosa* ATCC 9027 in the biofilm compared to the untreated group ($p = 0.042$). However, the colony-forming unit count was not significantly different between the treated groups. It is suggested that the combination of nanomaterials and antibiotics did not reduce the bacterial load in the biofilm more than nanomaterials alone. According to the previous study, the analysis of bacterial biofilm using the sonication method is influenced by the detachment of the bacterial cells from the surface, the count of colony-forming units, and the stage of detached bacterial biofilms. Therefore, quantification is limited to viable and cultivable bacterial cells [28].

This study had certain limitations. First, the antibiofilm activity of meropenem 1 mg/mL alone was not evaluated in this study, therefore the synergistic effect with meropenem could not be confirmed. Second, the structure of the biofilm involved was not described quantitively, including analysis of thickness variability, roughness coefficient, substratum coverage, and surface-to-volume ratio [39]. Further experiments using confocal imaging and the COMSTAT program are necessary to validate the results.

5. Conclusions

In summary, our study highlights the potential of employing combination therapies involving GlcN-AuNPs 0.02 mg/mL in conjunction with meropenem 1 mg/mL, as opposed to relying solely on antibiotics. Our findings underscore the enhanced antibacterial and antibiofilm efficacy achieved with the combination of GlcN-AuNPs and meropenem, presenting a successful strategy to counter the emerging resistance of *P. aeruginosa* to carbapenems. This approach aims to mitigate the risk of increased resistance, thereby reducing the higher morbidity and mortality resulting from treatment failures. Further investigation with quantitative analysis is necessary to confirm the synergistic effect between GlcN-AuNPs and meropenem.

Author Contributions: Conceptualization, D.S. and A.B.; methodology, D.S. and A.B.; formal analysis, D.S.; investigation, R.F.P., Y.M., S.P., L.D., H.A. and Y.L.N.; resources, D.S. and A.B.; data curation, D.S.; writing—original draft preparation, D.S. and Y.M.; writing—review and editing, D.S., A.B., R.F.P. and Y.M.; supervision, D.S. and A.B.; project administration, D.S.; funding acquisition, D.S. and A.B. All authors have read and agreed to the published version of the manuscript.

Funding: This research and the APC was funded by the PROGRAM PENELITIAN KOLABORASI INDONESIA—21 PTNBH TAHUN ANGGARAN 2023 (Brawijaya University, grant number 801.12/UN10.C10/TU/2023).

Institutional Review Board Statement: Ethical review and approval were not applicable due to the study not involving humans or animals.

Informed Consent Statement: Not applicable.

Data Availability Statement: Data are contained within the article.

Acknowledgments: We are thankful to Wisnu Barlianto, the Dean of the Faculty of Medicine, Universitas Brawijaya, Malang, Indonesia, and Yuanita Mulyastuti, the Head of the Laboratory of Microbiology, Faculty of Medicine, Universitas Brawijaya, Malang, Indonesia, who facilitated our study.

Conflicts of Interest: There are no conflicts of interest reported by any of the authors in relation to this article.

References

1. Pecoraro, C.; Carbone, D.; Deng, D.; Cascioferro, S.M.; Diana, P.; Giovannetti, E. Biofilm Formation as Valuable Target to Fight against Severe Chronic Infections. *Curr. Med. Chem.* **2022**, *29*, 4307–4310. [CrossRef]
2. Mulcahy, L.R.; Isabella, V.M.; Lewis, K. *Pseudomonas aeruginosa* Biofilms in Disease. *Microb. Ecol.* **2014**, *68*, 1–12. [CrossRef]
3. Pecoraro, C.; Carbone, D.; Parrino, B.; Cascioferro, S.; Diana, P. Recent Developments in the Inhibition of Bacterial Adhesion as Promising Anti-Virulence Strategy. *Int. J. Mol. Sci.* **2023**, *24*, 4872. [CrossRef]
4. Rachmawati, D.; Fahmi, M.Z.; Abdjan, M.I.; Wasito, E.B.; Siswanto, I.; Mazlan, N.; Rohmah, J.; Baktir, A. In Vitro Assessment on Designing Novel Antibiofilms of *Pseudomonas aeruginosa* Using a Computational Approach. *Molecules* **2022**, *27*, 8935. [CrossRef]
5. Tenke, P.; Köves, B.; Nagy, K.; Hultgren, S.J.; Mendling, W.; Wullt, B.; Grabe, M.; Wagenlehner, F.M.E.; Cek, M.; Pickard, R.; et al. Update on Biofilm Infections in the Urinary Tract. *World J. Urol.* **2012**, *30*, 51–57. [CrossRef]
6. Thi, M.T.T.; Wibowo, D.; Rehm, B.H. *Pseudomonas aeruginosa* Biofilms. *Int. J. Mol. Sci.* **2020**, *21*, 8671. [CrossRef]
7. Shineh, G.; Mobaraki, M.; Perves Bappy, M.J.; Mills, D.K. Biofilm Formation, and Related Impacts on Healthcare, Food Processing and Packaging, Industrial Manufacturing, Marine Industries, and Sanitation—A Review. *Appl. Microbiol.* **2023**, *3*, 629–665. [CrossRef]
8. Olejnickova, K.; Hola, V.; Ruzicka, F. Catheter-Related Infections Caused by *Pseudomonas aeruginosa*: Virulence Factors Involved and Their Relationships. *Pathog. Dis.* **2014**, *72*, 87–94. [CrossRef]
9. Cerioli, M.; Batailler, C.; Conrad, A.; Roux, S.; Perpoint, T.; Becker, A.; Triffault-Fillit, C.; Lustig, S.; Fessy, M.H.; Laurent, F.; et al. *Pseudomonas aeruginosa* Implant-Associated Bone and Joint Infections: Experience in a Regional Reference Center in France. *Front. Med.* **2020**, *7*, 513242. [CrossRef] [PubMed]
10. Hotterbeekx, A.; Xavier, B.B.; Bielen, K.; Lammens, C.; Moons, P.; Schepens, T.; Ieven, M.; Jorens, P.G.; Goossens, H.; Kumar-Singh, S.; et al. The Endotracheal Tube Microbiome Associated with *Pseudomonas aeruginosa* or *Staphylococcus epidermidis*. *Sci. Rep.* **2016**, *6*, 36507. [CrossRef] [PubMed]
11. Dargahi, Z.; Hamad, A.A.; Sheikh, A.F.; Khosravi, N.A.; Fard, S.S.; Motahar, M.; Mehr, F.J.; Abbasi, F.; Meghdadi, H.; Bakhtiyariniya, P.; et al. The Biofilm Formation and Antibiotic Resistance of Bacterial Profile from Endotracheal Tube of Patients Admitted to Intensive Care Unit in Southwest of Iran. *PLoS ONE* **2022**, *17*, e0277329. [CrossRef]

12. Sharma, S.; Mohler, J.; Mahajan, S.D.; Schwartz, S.A.; Bruggemann, L.; Aalinkeel, R. Microbial Biofilm: A Review on Formation, Infection, Antibiotic Resistance, Control Measures, and Innovative Treatment. *Microorganisms* **2023**, *11*, 1614. [CrossRef]
13. Shrestha, L.; Fan, H.M.; Tao, H.R.; Huang, J.D. Recent Strategies to Combat Biofilms Using Antimicrobial Agents and Therapeutic Approaches. *Pathogens* **2022**, *11*, 292. [CrossRef]
14. Sanya, D.R.A.; Onésime, D.; Vizzarro, G.; Jacquier, N. Recent Advances in Therapeutic Targets Identification and Development of Treatment Strategies towards *Pseudomonas aeruginosa* Infections. *BMC Microbiol.* **2023**, *23*, 86. [CrossRef]
15. Vital-Lopez, F.G.; Reifman, J.; Wallqvist, A. Biofilm Formation Mechanisms of *Pseudomonas aeruginosa* Predicted via Genome-Scale Kinetic Models of Bacterial Metabolism. *PLoS Comput. Biol.* **2015**, *11*, e1004452. [CrossRef]
16. Tran, H.M.; Tran, H.; Booth, M.A.; Fox, K.E.; Nguyen, T.H.; Tran, N.; Tran, P.A. Nanomaterials for Treating Bacterial Biofilms on Implantable Medical Devices. *Nanomaterials* **2020**, *10*, 2253. [CrossRef]
17. Pericolini, E.; Colombari, B.; Ferretti, G.; Iseppi, R.; Ardizzoni, A.; Girardis, M.; Sala, A.; Peppoloni, S.; Blasi, E. Real-Time Monitoring of *Pseudomonas aeruginosa* Biofilm Formation on Endotracheal Tubes in Vitro. *BMC Microbiol.* **2018**, *18*, 84. [CrossRef]
18. Hu, X.; Zhang, Y.; Ding, T.; Liu, J.; Zhao, H. Multifunctional Gold Nanoparticles: A Novel Nanomaterial for Various Medical Applications and Biological Activities. *Front. Bioeng. Biotechnol.* **2020**, *8*, 990. [CrossRef]
19. Su, C.; Huang, K.; Li, H.H.; Lu, Y.G.; Zheng, D.L. Antibacterial Properties of Functionalized Gold Nanoparticles and Their Application in Oral Biology. *J. Nanomater.* **2020**, *2020*, 5616379. [CrossRef]
20. Dykman, L.; Khlebtsov, N. Gold Nanoparticles in Biology and Medicine: Recent Advances and Prospects. *Acta Naturae* **2011**, *3*, 34–55. [CrossRef]
21. Taşkın Kafa, A.H.; Hasbek, M. Synergistic Efficacy of Meropenem, Ciprofloxacin and Colistin Antibiotics against Planktonic and Biofilm Forms of Myroides Odoratimimus Bacterial Isolates. *Indian J. Med. Microbiol.* **2022**, *40*, 399–403. [CrossRef]
22. Thorn, C.; Wignall, A.; Kopecki, Z.; Kral, A.; Prestidge, C.A.; Nicky, T. Liquid Crystal Nanoparticles Enhance Tobramycin Efficacy in a Murine Model of *Pseudomonas aeruginosa* Biofilm Wound Infection. *ACS Infect. Dis.* **2022**, *8*, 841–854. [CrossRef]
23. León-Buitimea, A.; Garza-Cárdenas, C.R.; Román-García, M.F.; Ramírez-Díaz, C.A.; Ulloa-Ramírez, M.; Morones-Ramírez, J.R. Nanomaterials-Based Combinatorial Therapy as a Strategy to Combat Antibiotic Resistance. *Antibiotics* **2022**, *11*, 794. [CrossRef]
24. Zhao, Y.; Wang, Z.; Zhang, W.; Jiang, X. Adsorbed Tween 80 Is Unique in Its Ability to Improve the Stability of Gold Nanoparticles in Solutions of Biomolecules. *Nanoscale* **2010**, *2*, 2114–2119. [CrossRef]
25. Govindaraju, S.; Ramasamy, M.; Baskaran, R.; Ahn, S.J.; Yun, K. Ultraviolet Light and Laser Irradiation Enhances the Antibacterial Activity of Glucosamine-Functionalized Gold Nanoparticles. *Int. J. Nanomedicine* **2015**, *10*, 67–78. [CrossRef]
26. Harika, K.; Shenoy, V.; Narasimhaswamy, N.; Chawla, K. Detection of Biofilm Production and Its Impact on Antibiotic Resistance Profile of Bacterial Isolates from Chronic Wound Infections. *J. Glob. Infect. Dis.* **2020**, *12*, 129–134. [CrossRef]
27. Swedan, S.; Shubair, Z.; Almaaytah, A. Synergism of Cationic Antimicrobial Peptide WLBU2 with Antibacterial Agents against Biofilms of Multi-Drug Resistant *Acinetobacter baumannii* and *Klebsiella pneumoniae*. *Infect. Drug Resist.* **2019**, *12*, 2019–2030. [CrossRef]
28. Mandakhalikar, K.D.; Rahmat, J.N.; Chiong, E.; Neoh, K.G.; Shen, L.; Tambyah, P.A. Extraction and Quantification of Biofilm Bacteria: Method Optimized for Urinary Catheters. *Sci. Rep.* **2018**, *8*, 8069. [CrossRef]
29. El-Telbany, M.; Mohamed, A.A.; Yahya, G.; Abdelghafar, A.; Abdel-Halim, M.S.; Saber, S.; Alfaleh, M.A.; Mohamed, A.H.; Abdelrahman, F.; Fathey, H.A.; et al. Combination of Meropenem and Zinc Oxide Nanoparticles; Antimicrobial Synergism, Exaggerated Antibiofilm Activity, and Efficient Therapeutic Strategy against Bacterial Keratitis. *Antibiotics* **2022**, *11*, 1374. [CrossRef]
30. Chen, X.; Ling, X.; Liu, G.; Xiao, J. Antimicrobial Coating: Tracheal Tube Application. *Int. J. Nanomedicine* **2022**, *17*, 1483–1494. [CrossRef]
31. Alonso, B.; Fernández-Barat, L.; Di Domenico, E.G.; Marín, M.; Cercenado, E.; Merino, I.; de Pablos, M.; Muñoz, P.; Guembe, M. Characterization of the Virulence of *Pseudomonas aeruginosa* Strains Causing Ventilator-Associated Pneumonia. *BMC Infect. Dis.* **2020**, *20*, 909. [CrossRef]
32. Pang, Z.; Raudonis, R.; Glick, B.R.; Lin, T.J.; Cheng, Z. Antibiotic Resistance in *Pseudomonas aeruginosa*: Mechanisms and Alternative Therapeutic Strategies. *Biotechnol. Adv.* **2019**, *37*, 177–192. [CrossRef] [PubMed]
33. Çiçek, A.Ç.; Ertürk, A.; Ejder, N.; Rakici, E.; Kostakoğlu, U.; Yıldız, İ.E.; Özyurt, S.; Sönmez, E. Screening of Antimicrobial Resistance Genes and Epidemiological Features in Hospital and Community-Associated Carbapenem-Resistant *Pseudomonas aeruginosa* Infections. *Infect. Drug Resist.* **2021**, *14*, 1517–1526. [CrossRef]
34. Wang, L.; Hu, C.; Shao, L. The Antimicrobial Activity of Nanoparticles: Present Situation and Prospects for the Future. *Int. J. Nanomedicine* **2017**, *12*, 1227–1249. [CrossRef]
35. Fernández-Gómez, P.; Pérez de la Lastra Aranda, C.; Tosat-Bitrián, C.; Bueso de Barrio, J.A.; Thompson, S.; Sot, B.; Salas, G.; Somoza, Á.; Espinosa, A.; Castellanos, M.; et al. Nanomedical Research and Development in Spain: Improving the Treatment of Diseases from the Nanoscale. *Front. Bioeng. Biotechnol.* **2023**, *11*, 1191327. [CrossRef]
36. Ali, S.G.; Ansari, M.A.; Alzohairy, M.A.; Alomary, M.N.; Alyahya, S.; Jalal, M.; Khan, H.M.; Asiri, S.M.M.; Ahmad, W.; Mahdi, A.A.; et al. Biogenic Gold Nanoparticles as Potent Antibacterial and Antibiofilm Nano-Antibiotics against *Pseudomonas aeruginosa*. *Antibiotics* **2020**, *9*, 100. [CrossRef]
37. Martínez, Á.; Lyu, Y.; Mancin, F.; Scrimin, P. Glucosamine Phosphate Induces AuNPs Aggregation and Fusion into Easily Functionalizable Nanowires. *Nanomaterials* **2019**, *9*, 622. [CrossRef]

38. Sicard, J.F.; Vogeleer, P.; Le Bihan, G.; Rodriguez Olivera, Y.; Beaudry, F.; Jacques, M.; Harel, J. N-Acetyl-Glucosamine Influences the Biofilm Formation of *Escherichia coli*. *Gut Pathog.* **2018**, *10*, 26. [CrossRef] [PubMed]
39. Heydorn, A.; Nielsen, A.T.; Hentzer, M.; Sternberg, C.; Givskov, M.; Ersboll, B.K.; Molin, S. Quantification of Biofilm Structures by the Novel Computer Program COMSTAT. *Microbiology* **2000**, *146*, 2395–2407. [CrossRef] [PubMed]